Experimental Neurology 320 (2019) 112964

Contents lists available at ScienceDirect

Experimental Neurology

journal homepage: www.elsevier.com/locate/yexnr

Research paper

Temporal changes in neuroinflammation and brain glucose metabolism in a rat model of viral vector-induced α-synucleinopathy

Melissa Crabbé[a,b,*], Anke Van der Perren[c,e], Savannah Kounelis[a,b], Thomas Lavreys[a,b], Guy Bormans[d], Veerle Baekelandt[b,c,e], Cindy Casteels[a,b], Koen Van Laere[a,b]

[a] Nuclear Medicine and Molecular Imaging, Department of Imaging and Pathology, KU Leuven, University Hospitals Leuven, Leuven, Belgium
[b] MoSAIC - Molecular Small Animal Imaging Centre, KU Leuven, Leuven, Belgium
[c] Laboratory for Neurobiology and Gene Therapy, Department of Neurosciences, KU Leuven, Leuven, Belgium
[d] Radiopharmaceutical Research, Department of Pharmaceutical and Pharmacological Sciences, KU Leuven, Leuven, Belgium
[e] Leuven Viral Vector Core, KU Leuven, Leuven, Belgium

ARTICLE INFO

Keywords:
Small-animal PET
Parkinson's disease
α-Synuclein
Translocator protein
Cerebral glucose metabolism

ABSTRACT

Rat models based on viral vector-mediated overexpression of α-synuclein are regarded as highly valuable models that closely mimic cardinal features of human Parkinson's disease (PD) such as L-DOPA-dependent motor impairment, dopaminergic neurodegeneration and α-synuclein inclusions. To date, the downstream effects of dopaminergic cell loss on brain glucose metabolism, including the neuroinflammation component, have not been phenotyped in detail for this model. Cerebral glucose metabolism was monitored throughout different stages of the disease using *in vivo* 2-[^{18}F]-fluoro-2-deoxy-D-glucose ([^{18}F]FDG) positron emission tomography (PET) and was combined with *in vitro* [^{18}F]DPA-714 autoradiography to assess concomitant inflammation. Rats were unilaterally injected with recombinant adeno-associated viral vector serotype 2/7 (rAAV2/7) encoding either A53T α-synuclein or eGFP. Brain [^{18}F]FDG microPET was performed at baseline, 1, 2, 3, 4, 6, and 9 weeks post-surgery, in combination with behavioral tests. As a second experiment, [^{18}F]DPA-714 autoradiography was executed across the same timeline. Voxel-based analysis of relative [^{18}F]FDG uptake showed a dynamic pattern of PD-related metabolic changes throughout the disease progression (weeks 2–9). Glucose hypermetabolism covering a large bilateral area reaching from the insular, motor- and somatosensory cortex to the striatum was observed at week 2. At week 4, hypermetabolism presented in a cluster covering the ipsilateral nigra-thalamic region, whereas hypometabolism was noted in the ipsilateral striatum at week 6. Elevated [^{18}F]FDG uptake was seen in a cluster extending across the contralateral striatum, motor- and somatosensory cortex at week 9. Increased [^{18}F]FDG in the region of the substantia nigra was associated with increased [^{18}F]DPA-714 binding, and correlated significantly with motor symptoms. These findings point to disease-associated metabolic and neuroinflammatory changes taking place in the primary area of dopaminergic neurodegeneration but also closely interconnected motor and somatosensory brain regions.

1. Introduction

The pathology of Parkinson's disease (PD) is characterized by to the progressive loss of dopaminergic neurons in the substantia nigra pars compacta (SN_c) (Poewe et al., 2017). This specific degeneration is related to the underlying α-synucleinopathy, for which dopaminergic neurons appear to be particularly vulnerable (Peelaerts et al., 2015). Additional pathological mechanisms have been identified, such as neuroinflammation, which could be either an early-stage event or a consequence of neuronal dysfunction (Eckert et al., 2007; Moehle and West, 2015; Ransohoff, 2016).

2-[^{18}F]-fluoro-2-deoxy-D-glucose ([^{18}F]FDG) allows the determination of regional glucose uptake, which is composed of the metabolic signature from both neurons and glial cells (Dienel et al., 2018; Wienhard, 2002; Zimmer et al., 2017). [^{18}F]FDG-PET studies in PD patients have identified specific PD-related brain patterns (PDRPs) that are correlated with prodromal PD and progressive motor- and cognitive symptomatology (Blum et al., 2018; Meyer et al., 2017; Walker et al., 2018). In rodents and non-human primates, various PD models are available, ranging from acute neurotoxin models to more progressive viral vector models that often more reliably mimic the human condition. Aberrant glucose metabolism in PD-associated brain regions was

* Corresponding author at: O&N 1 Herestraat 49 box 505, 3000 Leuven, Belgium.
E-mail address: melissa.crabbe@kuleuven.be (M. Crabbé).

https://doi.org/10.1016/j.expneurol.2019.112964
Received 14 March 2019; Received in revised form 9 May 2019; Accepted 22 May 2019
Available online 25 May 2019

shown in toxin-induced rodent models (Casteels et al., 2008; Im et al., 2016), but, to the best of our knowledge, no studies have been performed yet in more clinically relevant viral vector-based Parkinsonian models.

As mentioned previously, the [^{18}F]FDG signal originates from neuronal as well as glial cells in the brain. This implies that indirect changes to [^{18}F]FDG uptake due to localized inflammation cannot be interpreted as a marker for imaging of inflammation (Wu et al., 2013). Therefore, neuroinflammation imaging has mainly relied on more specific radioligands that bind molecules (in)directly connected to inflammatory processes, such as the translocator protein (TSPO). This 18-kDa protein is located on the outer mitochondrial membrane and has low expression rates under physiological conditions. Increased levels of TSPO binding have been observed in regions with reactive micro- and astrogliosis following several neuropathological conditions, including traumatic brain injury and stroke (Maia et al., 2012; Takkinen et al., 2017; Toth et al., 2016; Wang et al., 2014). In neurodegenerative disorders such as PD, conflicting data have been observed where the outcome is dependent on the utilized tracer and patient cohort (Bartels et al., 2010; Edison et al., 2013; Ghadery et al., 2017; Koshimori et al., 2015; Varnas et al., 2019).

To deepen our comprehension of the molecular mechanisms underlying PD and to validate new therapeutic strategies, continuous advances in animal models are indispensable. By means of viral vector technology, a robust and reproducible PD model was developed, overexpressing mutant or wild-type α-synuclein in the substantia nigra (SN) of rodents (Oliveras-Salva et al., 2013; Van der Perren et al., 2015b). This model encompasses both the slower timing of disease onset, symptom development and histopathological hallmarks of PD, and may be a better option for testing of novel therapeutic strategies. In humans, [^{18}F]FDG PET has been readily advocated to monitor therapeutic response (*e.g.* gene therapy, deep brain stimulation) (Chen et al., 2018; Niethammer et al., 2018).

In this study, we investigated the cerebral glucose metabolism pattern in the recombinant adeno-associated viral vector serotype 2/7 (rAAV2/7) A53T α-synuclein rat model using longitudinal [^{18}F]FDG microPET, in parallel with motor performance tests. Secondly, we assessed the potential relationship between metabolic changes and inflammation, as evaluated with *in vitro* [^{18}F]DPA-714 autoradiography.

2. Materials & methods

2.1. Study design

In this study, we evaluated the effect of unilateral viral vector-mediated A53T α-synuclein overexpression on cerebral glucose metabolism and neuroinflammation over time. In a first experiment, rats were subjected to baseline [^{18}F]FDG PET scans and behavioral tests, approximately one week prior to stereotactic surgery. Following stereotactic surgery, PET scans and behavioral tests (cylinder test and catwalk) were repeated at 1, 2, 3, 4, 6, and 9 weeks, based on previous observations of disease progression (Van der Perren et al., 2015b).

In a second experiment, we examined neuroinflammation using *in vitro* TSPO autoradiography with the [^{18}F]DPA-714 radioligand. This way we could visualize [^{18}F]DPA-714 binding with high resolution and sensitivity, in order to investigate small anatomical regions such as the SN, and also increase our output per radiotracer batch. An additional cohort of animals was included at 4 days, 2, 4, 6, and 9 weeks post-injection, and were evaluated for limb-use asymmetry using the cylinder test.

2.2. rAAV2/7 A53T α-synuclein rat model

All animal experiments were executed in accordance with the European Communities Council Directive 2010/63/EU and were approved by the local Animal Ethics Committee of the KU Leuven. Thirty-four female Wistar rats were injected with rAAV2/7 overexpressing α-synuclein harboring the A53T mutation (α-SYN; $n = 10$ for *in vivo* PET study; n = 24 for autoradiography). An equal number of control rats were unilaterally injected with rAAV2/7 expressing enhanced green fluorescent protein (eGFP). Rats were on average 8 weeks old, with a body weight range of 192–243 g. Animals had free access to pellet food and tap water and were under a 12 h light/dark cycle.

Vector production and purification, including stereotactic injections into the SN_c were executed as previously described (Van der Perren et al., 2015b). In short, animals were injected with 3 µl rAAV2/7 encoding A53T α-synuclein or eGFP (9.0 E + 11 genome copies (GC)/ mL vector dose). The following coordinates for the SN_c were used: anteroposterior (AP)-5.3, lateral (LAT)-2.0, dorsoventral (DV)-7.2.

2.3. Small-animal PET imaging and analysis

Imaging of cerebral glucose metabolism was performed using [^{18}F]FDG, which was synthesized in a standard synthesis module (IBA, Louvain-La-Neuve, Belgium). PET experiments were performed on a small-animal PET system (FOCUS-220; Siemens/Concorde Microsystems, Knoxville, TN, USA) with a 1.35 mm full-width at half-maximum (FWHM) transaxial resolution. Data were collected in a 128 × 128 × 95 matrix with a pixel width of 0.475 mm and 0.795 mm slice thickness. Tail veins were catheterized for injection of 22.0 ± 3.0 MBq [^{18}F]FDG (specific activity range 83–760 GBq/µmol). Before and during PET imaging, rodents were anesthetized using 2.0% isoflurane in 100% oxygen (1.5 l/min flow rate) and temperature was maintained at ± 37 °C. Static 30 min acquisitions were performed 60 min post-injection, after overnight fasting, as previously described (Casteels et al., 2006).

2.4. PET image reconstruction and data processing

List-mode data were reconstructed in a single frame using an iterative maximum a posterior probability (MAP) algorithm with ordered subsets (18 iterations, 9 subsets; fixed spatial resolution: 1.5 mm) and attenuation correction by means of a ^{57}Co attenuation scan that was acquired immediately before the static emission scan.

PET images were spatially normalized to a custom-made FDG rat brain template in Paxinos stereotactic space (Casteels et al., 2006). [^{18}F]FDG data were count normalized to the whole-brain uptake to determine the relative regional glucose metabolism (Spangler-Bickell et al., 2016).

Relative [^{18}F]FDG uptake images were analyzed by using a template-based volume of interest (VOI) approach (PMOD, v3.7, PMOD Technologies LTD, Zurich, Switzerland). Subsequently we utilized a voxel-by-voxel approach to obtain maximal use of information without *a priori* knowledge, using Statistical Parametric Mapping 12 (SPM12, Wellcome Department of Cognitive Neurology, London, United Kingdom). In short, we used a flexible factorial design depending on time point (baseline, 1, 2, 3, 4, 6, and 9 weeks) and group (eGFP or α-SYN), as described previously (Crabbe et al., 2018). T-maps were interrogated at a $p_{height} \leq 0.005$ (uncorrected) peak level and extend threshold of $k_E > 200$ voxels (1.6 mm^3). Only significant clusters with $p_{height} < 0.05$ (corrected for multiple comparisons) were retained.

2.5. In vitro [^{18}F]DPA-714 autoradiography

Rats were sacrificed at 4 days, 2, 4, 6, and 9 weeks after viral vector injection, the cerebrum was excised, and rapidly frozen in 2-methylbutane (−30 °C until −40 °C). After cryosectioning, 20 µm transversal sections were mounted and stored at −80 °C. *In vitro* autoradiography was executed following the protocol described by Ory et al. (2016). In short, after pre-incubation, brain slices were incubated for 10 min with 596 kBq/slice of [^{18}F]DPA-714 tracer solution. Non-specific binding was assessed on consecutive sections in conjugation with 20 µM PK-

11195 (Sigma-Aldrich, St. Louis, MO, USA) as a blocking agent. Following washing steps, slides were exposed to a phosphor storage screen to obtain autoradiograms. Radioactivity concentration in the autoradiograms is indicated as digital light units (DLU) per square millimeter (mm^2). Region-of-interest (ROI) analyses of the obtained autoradiograms were performed to quantify TSPO binding in the substantia nigra and striatum. A minimum of 4 transverse slices throughout the ROI were included per animal. ROIs were manually delineated and mean ligand binding minus background binding was calculated. In our analyses, the contralateral ROIs served as a reference region, in accordance with previous TSPO research (Maia et al., 2012; Ory et al., 2016; Wang et al., 2014). Therefore, data are represented as binding ratios of the DLU/mm^2 in the ipsi- to contralateral side.

2.6. Histology and stereological quantification

The perfusion procedure, tissue sectioning and tyrosine hydroxylase (TH) immunostaining were performed as described previously on brains of α-SYN and eGFP rats at 9 weeks post-injection (Van der Perren et al., 2015b). In short, 50 µm floating sections were incubated with rabbit anti-tyrosine hydroxylase (TH) antibody (1:1000, rabbit polyclonal, AB152, Sigma) followed by biotinylated anti-rabbit IgG (1:300, Agilent, Santa Clara, CA, USA) and streptavidin-horseradish peroxidase complex (1:1000, Agilent). Serial sections throughout the SN were analyzed at a 200 µm interval (between approximately −4.56 until −6.12 AP), with a minimum of 7 sections for each animal. Quantification of TH-positive neurons in the SN_c was performed by using the optical fractionator method (StereoInvestigator, MicroBrightField, Magdeburg, Germany) (Baekelandt et al., 2002).

2.7. Behavioral testing

Motor function was evaluated using the cylinder and CatWalk test and were chosen because of their ability to detect motor symptoms in the rAAV2/7 α-synuclein model (Van der Perren et al., 2015b).

2.7.1. The limb-use asymmetry (cylinder) test

The cylinder test was performed to longitudinally assess the asymmetry of spontaneous forelimb use during explorative activity as a surrogate marker for DA degeneration and quantification of TH+ cells. Rats were allowed to explore a transparent glass cylinder (20 cm diameter) for 5 min, which was videotaped for analysis. The number of wall contacts by either left or right limb were counted per rat until a minimum of 20 contacts was recorded. Simultaneous contacts with both limbs were excluded and only supporting contacts were counted. Wall contacts were expressed as percentage wall contacts of the affected forelimb relative to the total number of contacts (% I). Given that the cylinder test was performed at identical time points in both *in vivo* and *in vitro* imaging cohorts, data were merged for analysis.

2.7.2. CatWalk

Using the CatWalk (Noldus Information Technology, Wageningen, The Netherlands), we evaluated gait disturbances over time, looking at different measures, including amongst others: print width, print intensity, stride length and interlimb coordination. The principle of this technique relies upon optical reflection of paw contact points using a fluorescent tube. Training and assessment of rats was performed as described before (Crabbe et al., 2018). In short, we included the average performance out of 3 runs, with a minimum of 4 step sequences, for analysis.

2.8. General statistics

Reported values are described as the mean ± standard deviation. Statistics were carried out using Graphpad Prism 7 (Graphpad Software, La Jolla, CA, USA). VOI data and behavioral outcomes were analyzed using a 2-way repeated-measures analysis of variance (ANOVA) with 'time' and 'group' as between-subject factors. Non-repeated measures ANOVA was used for analysis of autoradiography readouts. An unpaired *t*-test was used to analyze TH-positive cell loss. Post-hoc tests were included for correction of multiple comparisons, *i.e.* Sidak tests for behavioral measures and autoradiography, and Bonferroni tests for TH immunostaining.. The Spearman's rank coefficient was utilized for correlative tests. P-values < 0.05 were accepted as statistically significant.

3. Results

3.1. Longitudinal [^{18}F]FDG PET imaging of brain glucose metabolism

VOI-based analysis did not indicate significant alterations. Relative [^{18}F]FDG uptake showed a dynamic pattern of regional metabolic changes involving different PD-associated regions, as indicated by voxel-wise analysis.

Two weeks after injection of the viral vector, rats from the α-SYN group presented with transiently elevated glucose uptake in a cluster covering the bilateral motor cortex, somatosensory cortex, and the striatum, as compared to eGFP rats (+33.4 ± 13.5% at the Paxinos coordinate peak maximum; $p_{uncorr} = 2.9*10^{-7}$; Figs. 1 & 2 A). At 4 weeks post-lesioning, a 10.0 ± 5.3% increase was found in a cluster covering the region of injection in the SN_c, extending to the thalamic

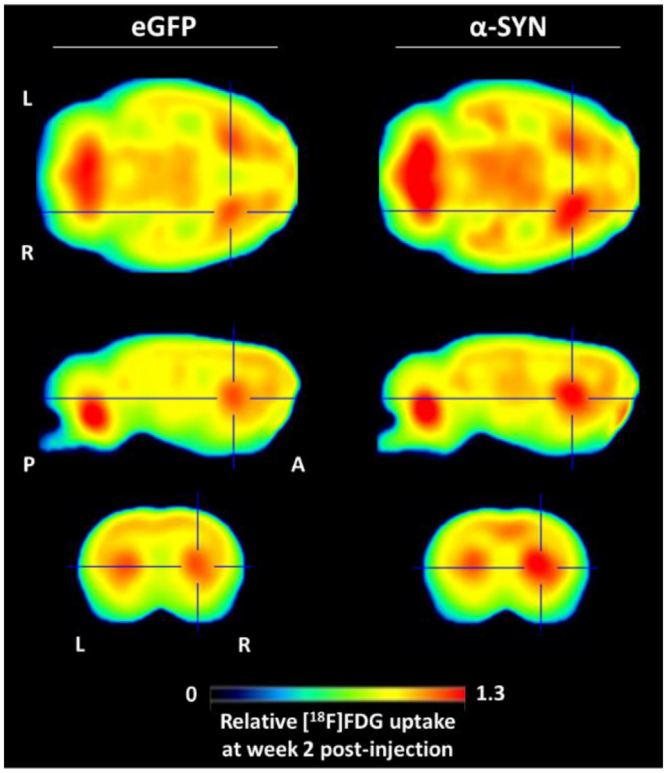

Fig. 1. *In vivo* [^{18}F]FDG PET imaging shows altered glucose metabolism associated with α-synucleinopathy. Average cross-sectional small-animal PET images of animals injected with viral vector overexpressing either mutant A53T α-synuclein or eGFP (controls), at 2 weeks post-injection, where the maximal difference in [^{18}F]FDG uptake was observed. Note the visually higher glucose uptake in the striatum ipsilateral to the injected α-SYN vector (right hemisphere) in comparison with the eGFP group, as indicated by the orthogonal crosshairs. Color bar indicates [^{18}F]FDG relative intensity. Abbreviations: [^{18}F]FDG, ^{18}F-fluorodeoxyglucose; α-SYN: α-synuclein group; eGFP, enhanced green fluorescent protein; PET, positron emission tomography; A, anterior; P, posterior; L, left; R, right. (For interpretation of the references to color in this figure legend, the reader is referred to the web version of this article.)

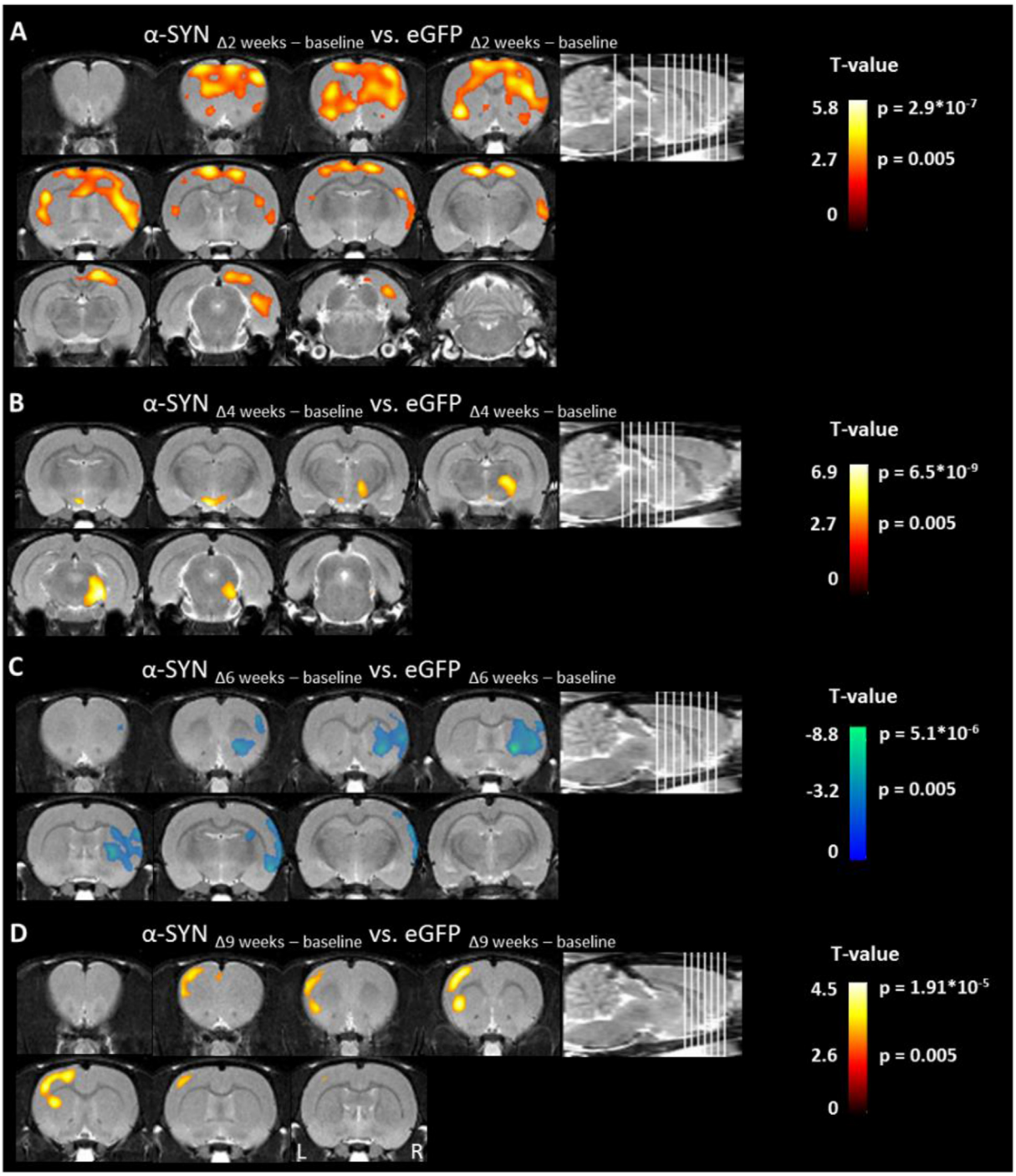

Fig. 2. rAAV2/7 A53T α-synuclein overexpression in the SN affects cerebral glucose metabolism in distinct cerebral regions over time, as shown by voxel-wise analysis. Coronal brain sections indicate overlays on the regions with significantly altered relative [^{18}F]FDG uptake at week 2 (A), week 4 (B), week 6 (C) and week 9 (D) after injection of the viral vector. Significant clusters are shown using a T-statistic color scale, which corresponds to the level of significance at the voxel level. Abbreviations: α-SYN: α-synuclein; eGFP, enhanced green fluorescent protein; L, left; R, right.

and raphe nucleus ($p_{uncorr} = 6.5*10^{-9}$; Fig. 2 B). This relative hypermetabolism remained present at week 6, though non-significant at the cluster level. At the same time point, α-SYN rats depicted reduced [^{18}F]FDG uptake in a cluster covering the ipsilateral somatosensory cortex and striatum (11.7 ± 3.4%; $p_{uncorr} = 5.1*10^{-6}$; Fig. 2C). Finally, 9 weeks into the experiment, α-SYN rats presented with 19% higher [^{18}F]FDG uptake in a cluster surrounding the contralateral motor- and somatosensory cortex, and the striatum ($p_{uncorr} = 1.9*10^{-5}$; Fig. 2 D). A detailed overview of cluster peak locations and intensities can be found in Table 1.

3.2. *In vitro* [^{18}F]DPA-714 autoradiography for the assessment of neuroinflammation

In order to interpret the plausible neuroinflammation component of the [^{18}F]FDG images, we performed *in vitro* autoradiography with the TSPO radioligand [^{18}F]DPA-714. α-SYN autoradiograms showed a focal increase of [^{18}F]DPA-714 binding in the ipsilateral SN across 4- and 6-week time points, as compared with the eGFP group ($p < .0001$), with a mean difference of +84 ± 17% at week 4 and + 71 ± 18% at week 6 (Fig. 3 A & C). Both treatment groups also showed focal radiotracer

Table 1
Peak locations and statistical details for the clusters obtained from the statistical parametric mapping analysis between the α-SYN and eGFP group. p_{corr}, p-value at cluster level, corrected for the investigated volume; K_E, cluster extent; T, measure of statistical significance; p_{uncorr}, p-value at the voxel level, uncorrected for the investigated volume; intensity difference (in percentage) at the voxel level between α-SYN rats and eGFP-overexpressing controls; x, lateral distance from the midline in millimeter (mm); y, anteroposterior location with Bregma as reference; z, dorsoventral location, coordinates based on the Paxinos stereotactic atlas; Wk, week; wk 0 indicates baseline measurements.

	Cluster level		Voxel level			Structure			
	p_{corr}	K_E	T	p_{uncorr}	Intensity difference (%)	x	y	z	Name
α-syn Δ(wk 2-wk 0) > eGFP Δ(wk 2-wk 0)	< 0.001	26,012	5.88 5.71 5.66	< 0.001 < 0.001 < 0.001	+33.4 ± 13.5	0.8 −4.0 4.0	−2.8 2.6 1.2	−1.2 −2.8 −6.8	Bilateral primary and secondary motor cortex, primary somatosensory, insular and agranular cortex, striatum
α-syn Δ(wk 4-wk 0) > eGFP Δ(wk 4-wk 0)	0.029	923	5.19 4.06 3.52	< 0.001 < 0.001 0.001	+10.0 ± 5.3	−2.4 −2.4 −0.8	−6.4 −5.4 −6.8	−6.8 −6.8 −7.6	Ipsilateral SN, posterior thalamic nuclei, raphe nuclei
α-syn Δ(wk 6-wk 0) < eGFP Δ(wk 6-wk 0)	< 0.001	7100	8.81 7.44 6.78	< 0.001 < 0.001 < 0.001	−11.7 ± 3.4	−2.6 −6.4 −4.4	0.0 −3.4 2.2	−6.6 −3.8 −3.2	Ipsilateral primary and secondary somatosensory cortex, striatum
α-syn Δ(wk 9-wk 0) > eGFP Δ(wk 9-wk 0)	< 0.001	2433	4.54 4.28 4.25	< 0.001 < 0.001 < 0.001	+19.0 ± 6.5	4.2 4.0 3.8	1.8 1.2 1.6	−6.0 −5.2 −2.2	Contralateral insular cortex, primary motor and somatsensory cortex, striatum

uptake along the needle track following stereotactic surgery, which disappeared in both groups over time. In contrast, tracer binding in the striatum was not significantly affected by α-synucleinopathy (p = .11), though a small between-group difference was observed over time, reaching significance at the 9-week time point (ipsi-to-contralateral binding ratio: 1.0 ± 0.1 *vs.* 1.1 ± 0.1, p = .015; Fig. 3 B–C).

3.3. Evaluation of dopaminergic cell loss and motor symptom development

Rats from the α-SYN group showed a significant decrease in the number of TH-positive cells, in comparison with the eGFP group at 9 weeks post-injection (773 ± 401 *vs.* 11,748 ± 2153 TH+ cells; Fig. 4 A–B). To evaluate deteriorating motor performance in rodents, we used the limb-use asymmetry and CatWalk tests, which analyze functional deficits in spontaneous forelimb use and gait.

α-SYN rats gradually developed limb-use asymmetry, with significant impairment of the contralateral forepaw starting from week 2 post-lesioning, as compared with eGFP rats (p < .001 at week 9; Fig. 4 C). The CatWalk motor test did not indicate any significant effects of α-synuclein A53T overexpression on main factors such as print width, print intensity, stride length and interlimb coordination, after correction for multiple testing (2-way ANOVA, p > .05; data not shown).

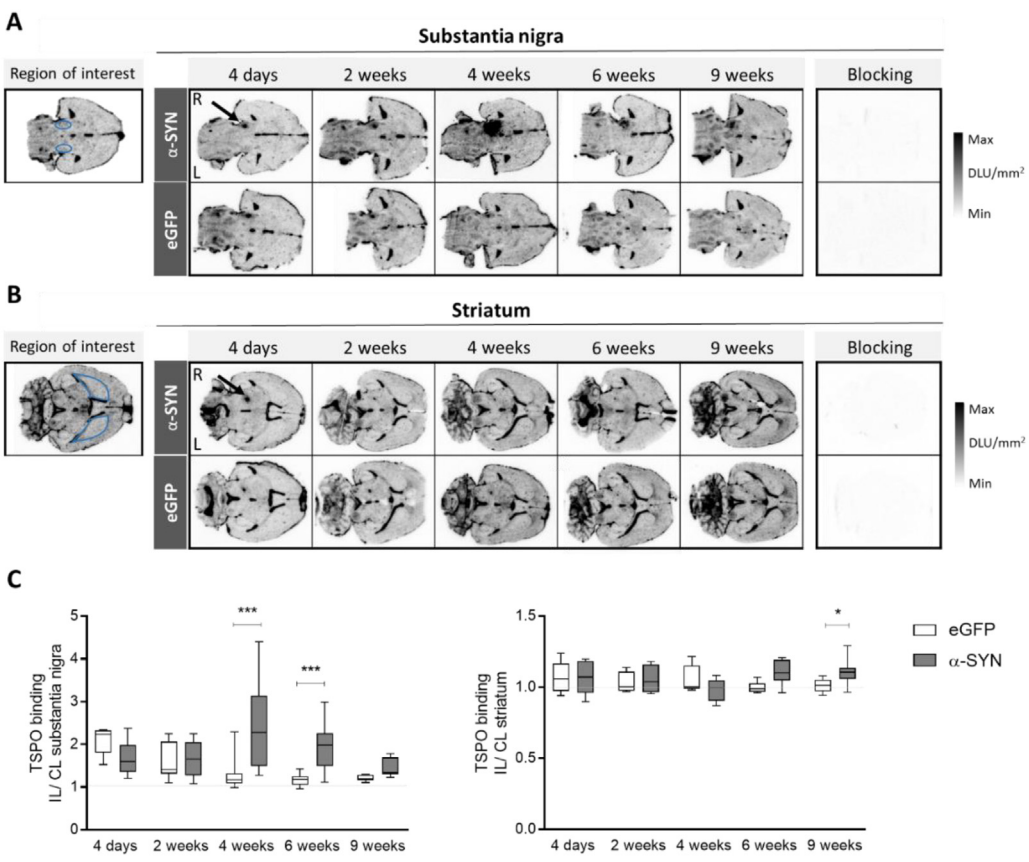

Fig. 3. TSPO availability is increased in the striatum and substantia nigra of α-SYN rats, as evaluated by *in vitro* autoradiography. Representative images of [^{18}F]DPA-714 autoradiograms in the SN (A) and striatum (B) across all time points and groups. The left plane highlights the delineated region-of-interest (ROI, blue). Images of PK-11195 blocking studies at the 4- and 9-week time point were included for nigral and striatal analyses, respectively. Black arrows indicate regions with increased [^{18}F]DPA-714 binding in the SN (A) and along the needle track (B). (C) Ipsi- to contralateral [^{18}F]DPA-714 binding ratios in the ROI are represented in box plots. N = 4–7 per group and per time point with ≥4 quantified brain slices throughout the ROI per animal. All slices are represented in the box plots. **p < .01, ***p < .001. 2-way ANOVA with Sidak post-hoc test. Abbreviations: ANOVA, analysis of variance; α-SYN, α-synuclein; DLU, digital light units; IL, ipsilateral; CL, contralateral; L, left; R, right. (For interpretation of the references to color in this figure legend, the reader is referred to the web version of this article.)

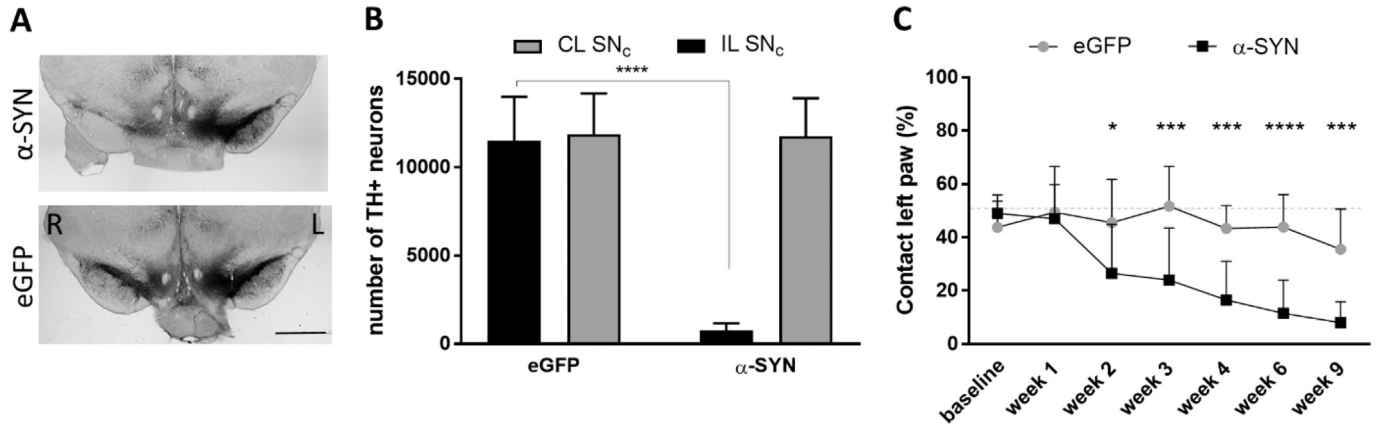

Fig. 4. Viral vector-induced A53T α-synuclein overexpression is characterized by dopaminergic cell loss in the SN and the gradual development of limb-use asymmetry. (A) A representative coronal section with tyrosine hydroxylase immunostaining shows dopaminergic cell loss in the ipsilateral SN of an α-SYN *versus* eGFP rat. Scale bar = 2000 μm (B) Stereological quantification of TH-positive cells in the SN_c. ****p < .0001, unpaired *t*-test with Bonferroni post-hoc test. (C) α-SYN rats develop significant limb-use asymmetry over time, as measured by the cylinder test. *p < .05, ***p < .001, ****p < .0001. 2-way ANOVA with Sidak post-hoc test. Abbreviations: α-SYN, α-synuclein; CL, contralateral; IL, ipsilateral; SN_c, substantia nigra pars compacta; TH, tyrosine hydroxylase; L, left; R, right.

3.4. Correlation analysis of in vivo [^{18}F]FDG uptake in the brain with behavioral outcome and dopaminergic cell loss in the SN

Limb-use asymmetry, measured at week 2, 3 and 4, was found to be correlated with dopaminergic cell loss in the affected SN_c at week 9 (W2: r = 0.80, p = .01; W3: r = 0.93, p < .001; W4: r = 0.84, p = .007; Fig. 5 A). This indicates that rats with a higher number of surviving TH+ cells maintained a better motor function, in accordance with previous research (Tillerson et al., 2001). An inverse relation was shown between limb-use asymmetry and peak relative [^{18}F]FDG uptake in a cluster covering the ipsilateral SN and thalamic area, both at week 4 (r = −0.93, p < .001; Fig. 5 B). Peak cluster values in the region of the ipsilateral striatum and cortex correlated positively with limb-use asymmetry, both at week 6 (r = 0.96; p < .001; Fig. 5 C). No other regional correlation was found between [^{18}F]FDG uptake, behavioral outcomes and TH+ neuronal cell loss. In the *in vitro* cohort, no significant correlation was found between limb-use asymmetry and nigral [^{18}F]DPA-714 binding.

4. Discussion

In an effort to improve the translational potential of preclinical PD models, new innovative transgenic and viral vector models have been developed. Measurements of regional glucose metabolism can aid to assess therapeutic responses in these models, but also to detect disease-associated patterns, which can give additional insight into the disease neurobiology. Our data show that α-synucleinopathy, mediated by rAAV2/7-mediated overexpression in the substantia nigra, led to an alternating hyper- and hypometabolic pattern in the rat cerebrum during the course of a 9-week period. Of these changes, we show that elevated [^{18}F]FDG uptake in the region of the SN corresponds to an inflammatory response, as shown by [^{18}F]DPA-714 autoradiography. Lastly, we describe a significant relation between motor function and relative [^{18}F]FDG uptake in the SN and striatum.

In this study, we report widely distributed changes to glucose uptake in the rAAV2/7 A53T α-synuclein model, which take place during consecutive stages of the neurodegenerative process (Van der Perren et al., 2015b). At the 2-week time point, hypermetabolism was observed mainly in the motor- and sensorimotor cortices including striatal regions. Previous reports indicated a major decline in DA-content (−60%) and TH-positive cell loss (~50%) and striatal [^{18}F]FECT binding at the same time point, pointing to a substantial loss of DAergic markers (Van der Perren et al., 2015b). Given that glucose is the primary energy source for neuronal activity, elevated [^{18}F]FDG uptake may reflect a compensatory increased neuronal function associated with disease (Dienel et al., 2018; Dienel and Hertz, 2001). A similar metabolic pattern was described in PD patients and MPTP non-human primates where elevated [^{18}F]FDG uptake was found in key regions of

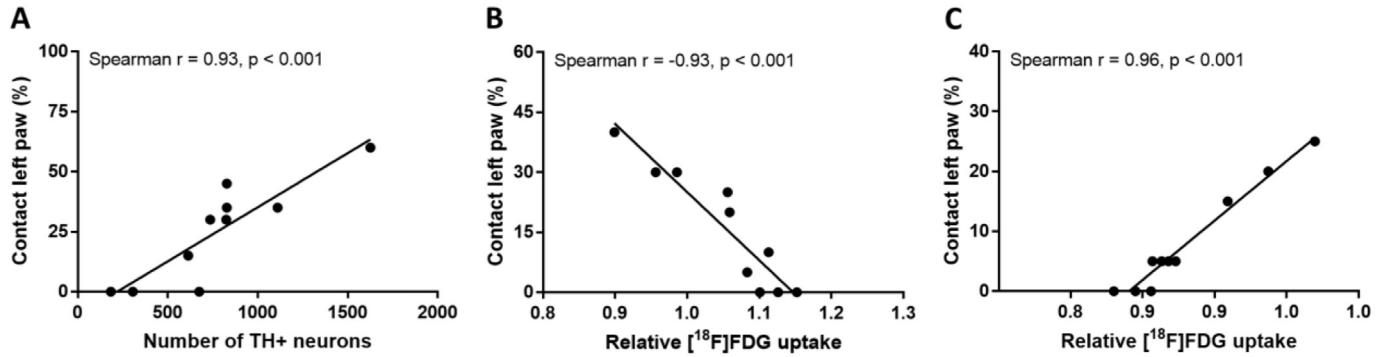

Fig. 5. Limb-use asymmetry is correlated with TH+ cell loss and regional alterations in glucose uptake. (A) The percentage of spontaneous contacts with the affected forepaw at week 4 was related to the number of remaining TH-positive cells in the ipsilateral SN_c at 9 weeks post-injection. (B–C) Scatter plots indicate relative [^{18}F]FDG uptake at the maximal peak value of the cluster in relation to limb-use asymmetry. (B) At 4 weeks post-injection, a negative correlation was present between limb-use asymmetry and peak cluster values in the region of the ipsilateral substantia nigra. (C) A positive correlation between limb-use asymmetry and peak cluster values covering the ipsilateral striatum and cortex at week 6. The correlation analysis was performed using the Spearman Log-rank test. Abbreviations: SN_c, substantia nigra pars compacta; TH, tyrosine hydroxylase.

the motor system including the basal ganglia and sensorimotor cortices (Ma et al., 2015; Schindlbeck and Eidelberg, 2018). However, all rodent PD PET studies have been performed in acute 6-OHDA models that, due to their acute degenerative pattern, make it difficult to compare disease stages. Compensatory mechanisms have been described in early-stage PD patients where axonal density increased in the cortico-basal-ganglia-thalamo-cortical loop suggesting adaptive neuroplasticity to counteract ongoing neurodegeneration (Mole et al., 2016).

In parallel with progressive synucleinopathy and further dopaminergic degeneration, we noted glucose hypermetabolism in the ipsilateral nigra-thalamic region. At this stage > 80% of the dopaminergic cells were degenerated, suggesting that increased [^{18}F]FDG uptake may originate from increased metabolic activity of the remaining cells present in SN or, alternatively, projection neurons originating from the subthalamic nucleus (Shimo and Wichmann, 2009; Van der Perren et al., 2015b). Given that rAAV2/7-mediated α-synuclein overexpression preferentially targets dopaminergic cells, remaining neurons may consist of (non-) dopaminergic neurons (*i.e.* striatonigral GABAergic nerve terminals or GABAergic nigra-thalamic projection neurons) or infiltrating microglial or astroglial cells. Of note, inflammation sites are generally marked by high glucose consumption and could mask regional metabolic decrements due to dopaminergic neurodegeneration (Wu et al., 2013). This hypothesis is supported by Zimmer and colleagues, who indicated that astroglial activity contributes significantly to the [^{18}F]FDG PET signal (Zimmer et al., 2017).

At week 6 and 9, we described striatal hypometabolism and cortical hypermetabolism in the ipsi- and contralateral hemisphere, respectively. These observations took place at a stage with advanced DAergic degeneration in the nigrostriatal pathway, as shown previously by DA transporter PET imaging and tyrosine hydroxylase immunostaining, and might more accurately reflect late-stage PD (Van der Perren et al., 2015b). Reduced [^{18}F]FDG uptake in the striatum may be a (in)direct effect of nigrostriatal deafferentation and has been extensively described in patients with advanced PD, as well as unilateral 6-OHDA rodent models (Casteels et al., 2008; Im et al., 2016; Jang et al., 2012; Walker et al., 2018). These results are supported by magnetic resonance spectroscopy (MRS) studies in the striatum of 6-OHDA-lesioned rodents, where decreased *N*-acetyl-aspartate levels have been attributed to the loss of nigrostriatal dopaminergic fibers (Coune et al., 2013).

Increased neuronal activity in the contralateral hemisphere may indicate a compensatory mechanism to restore the dysfunctional ipsilateral motor loop. Especially in rodents, adaptive neuroplasticity could recruit parallel motor circuits in an effort to normalize unilaterally injured or dysfunctional motor networks (Casteels et al., 2008; Guo et al., 2015).

Interestingly, clinically observed cognitive patterns, affecting the caudate nucleus, parietal and occipital cortex, were largely absent in this model (Meyer et al., 2017; Poewe et al., 2017). However, PD-related cognitive patterns in late-stage PD patients are associated with developing dementia and spreading of α-synucleinopathy outside of the midbrain, which have not been described in this model (Huang et al., 2007; Peelaerts et al., 2015; Van der Perren et al., 2015b).

In this study, isoflurane anesthesia was used during image acquisition. Isoflurane has a known effect on regional [^{18}F]FDG brain uptake though inclusion of both α-SYN and control groups should exclude possible effects of the anesthesia procedure (Spangler-Bickell et al., 2016). Moreover, isoflurane equally affected the regional cerebral metabolic rate of cortico-basal ganglia networks in both intact and DA-denervated hemispheres of 6-OHDA rats, as measured by [14C]-2-deoxyglucose autoradiography (Bimpisidis et al., 2017).

In correspondence with previous AAV research, nigral delivery of A53T mutant α-synuclein resulted in behavioral motor impairment and significant dopaminergic cell loss in the SN_c. As expected, rats showed spontaneous limb-use asymmetry concomitant with progressive DA impairment. Compared to other AAV or lentiviral models, which commonly do not reach > 50% reduction of TH-positive cells, the rAAV2/7 model does reach sufficient degeneration to reliably mimic PD-related symptoms also observed in patients (Decressac et al., 2012; Lauwers et al., 2007; Lo Bianco et al., 2002).

In accordance with PDRP's which generally correlate with the patients' motor symptom severity (Matthews et al., 2018; Meyer et al., 2017), we demonstrated a significant relation between limb-use asymmetry and regional [^{18}F]FDG uptake. A higher degree of motor impairment was related to elevated [^{18}F]FDG uptake in the region of injection, which might point to a link between neuroinflammation and motor function. We also found that the lowest levels of striatal FDG uptake were correlated to more severe motor deficits, resembling the impaired DAergic function in the striatum (Casteels et al., 2008; Im et al., 2016).

In an effort to disentangle the role of inflammatory processes in the brain, TSPO ligands have been most widely used, since TSPO is overexpressed by activated microglia and may reflect changes in the microglial phenotype (Banati, 2002; Chen and Guilarte, 2008). In our study, we opted to use *in vitro* autoradiography for assessment of TSPO binding because of its high sensitivity and resolution. We found increased *in vitro* [^{18}F]DPA-714 binding to the region of the ipsilateral substantia nigra in α-SYN rats. In line with the voxel-wise [^{18}F]FDG findings, these regional changes occurred in the same period, from 4 to 6 weeks post-injection. As reported before, high glucose turnover in immune cells could compensate decreased FDG uptake due to neurodegeneration (Takkinen et al., 2017). Indeed, a maximal number of CD11 b-positive activated microglia that depicted a cluster-forming pattern were previously shown in the transduced substantia nigra at week 4 (Van der Perren et al., 2015a). At this time point, microglia were positive for CD68 and major histocompatibility complex II (MHCII), both markers of microglial activation.

Aggregated (monomers to fibrils) α-synuclein can activate microglia and induce substantial inflammatory factor production, which in turn may induce neuronal death (Bruck et al., 2016). Activated microglia were found surrounding nigral neurons with cytoplasmic α-synuclein aggregates both in PD patients *post-mortem* as experimental models *ex vivo* (Chung et al., 2009; Gao et al., 2008; McGeer et al., 1988; Theodore et al., 2008). Not surprisingly, elevated TSPO binding has been extensively reported in acute PD models though we found no previous studies utilizing TSPO radioligands across subsequent disease stages in viral vector-based or transgenic PD models. Using different viral vector serotypes and titers, several authors reported an increase in activated microglia and pro-inflammatory cytokines surrounding the dopaminergic cell bodies and terminals at an early degenerative stage (Chung et al., 2009; Sanchez-Guajardo et al., 2010; Theodore et al., 2008). Our data revealed significant alterations from week 4, when the majority of nigral degeneration has already taken place, possibly reflecting a later disease stage. Of note, it remains difficult to compare time-specific effects between AAV models, due to the variability in disease progression and DAergic cell loss.

In clinical PD, TSPO binding was found increased (Iannaccone et al., 2013; Terada et al., 2016) as well as invariable (Ghadery et al., 2017; Koshimori et al., 2015; Varnas et al., 2019) using different radioligands and patient cohorts with various disease stage and severity. Increased TSPO binding was described in the midbrain and basal ganglia, extending towards to occipital, temporal and parietal cortex with disease progression (Edison et al., 2013; Iannaccone et al., 2013; Terada et al., 2016). Inflammatory processes are expected to vary with disease progression though it is unlikely that these inconsistent findings can be explained solely by heterogeneity of the examined patient cohorts. Also differences in (i) genotype-dependent tracer affinity, (ii) plasma protein binding, and (iii) quantification methodology possibly complicate the interpretation of TSPO PET studies in humans (Turkheimer et al., 2015).

In this experiment, both α-SYN and eGFP groups exhibited a limited inflammatory response along the needle trajectory, which subsided after 2 weeks following surgery. Minimal activation of microglia and/or

macrophages, including CD8+ T cells was reported in the SN of eGFP-transduced animals at this number of viral vector particles/copies (Van der Perren et al., 2015a). In addition, TH-positive cell counts remained unchanged in the eGFP group, indicating that control animals display no neuronal degeneration over time. This way we could distinguish between inflammatory reactions due to protein overexpression-mediated toxicity or the stereotactic surgery.

Together, our data demonstrated dynamic metabolic patterns in the rAAV2/7 A53T α-synuclein model throughout the course of the disease. Elevated [^{18}F]FDG uptake in the nigral region was related to a corresponding increase in [^{18}F]DPA-714 binding at late disease stages. We also found a relation between motor symptoms and altered [^{18}F]FDG uptake in the motor pathway, providing an additional link between neuroimaging and disease pathology. These results indicate the potential of [^{18}F]FDG PET imaging for follow-up of disease progression and evaluation of treatment response in future studies.

Acknowledgements

We thank Ann Van Santvoort for her excellent technical support and Annelies Aertgeerts for performing the stereotactic surgery. We also thank the PET radiopharmacy team of the University Hospitals Leuven for tracer preparations. Viral vectors were developed and produced by the Leuven Viral Vector Core (Leuven, Belgium). This work was supported by the European Commission, FP7, INMiND [grant agreement no. 278850], the Research Foundation – Flanders [G.0927.14 and G080517N], and KU Leuven Myriad project [OF/14/120]. Melissa Crabbé is a fellow of the Research Foundation – Flanders (FWO Vlaanderen). Cindy Casteels and Anke Van der Perren was/is supported by a postdoctoral mandate of the Research Foundation - Flanders. Koen Van Laere is a senior clinical investigator of the Research Foundation - Flanders.

Declarations of interest

None

References

Baekelandt, V., Claeys, A., Eggermont, K., Lauwers, E., De Strooper, B., Nuttin, B., Debyser, Z., 2002. Characterization of lentiviral vector-mediated gene transfer in adult mouse brain. Hum. Gene Ther. 13, 841–853.

Banati, R.B., 2002. Visualising microglial activation in vivo. Glia 40, 206–217.

Bartels, A.L., Willemsen, A.T., Doorduin, J., de Vries, E.F., Dierckx, R.A., Leenders, K.L., 2010. [11C]-PK11195 PET: quantification of neuroinflammation and a monitor of anti-inflammatory treatment in Parkinson's disease? Parkinsonism Relat. Disord. 16, 57–59.

Bimpisidis, Z., Oberg, C.M., Maslava, N., Cenci, M.A., Lundblad, C., 2017. Differential effects of gaseous versus injectable anesthetics on changes in regional cerebral blood flow and metabolism induced by l-DOPA in a rat model of Parkinson's disease. Exp. Neurol. 292, 113–124.

Blum, D., la Fougere, C., Pilotto, A., Maetzler, W., Berg, D., Reimold, M., Liepelt-Scarfone, I., 2018. Hypermetabolism in the cerebellum and brainstem and cortical hypometabolism are independently associated with cognitive impairment in Parkinson's disease. Eur. J. Nucl. Med. Mol. Imaging 45, 2387–2395.

Bruck, D., Wenning, G.K., Stefanova, N., Fellner, L., 2016. Glia and alpha-synuclein in neurodegeneration: a complex interaction. Neurobiol. Dis. 85, 262–274.

Casteels, C., Vermaelen, P., Nuyts, J., Van Der Linden, A., Baekelandt, V., Mortelmans, L., Bormans, G., Van Laere, K., 2006. Construction and evaluation of multitracer small-animal PET probabilistic atlases for voxel-based functional mapping of the rat brain. J. Nucl. Med. 47, 1858–1866.

Casteels, C., Lauwers, E., Bormans, G., Baekelandt, V., Van Laere, K., 2008. Metabolic-dopaminergic mapping of the 6-hydroxydopamine rat model for Parkinson's disease. Eur. J. Nucl. Med. Mol. Imaging 35, 124–134.

Chen, M.K., Guilarte, T.R., 2008. Translocator protein 18 kDa (TSPO): molecular sensor of brain injury and repair. Pharmacol. Ther. 118, 1–17.

Chen, H.M., Sha, Z.Q., Ma, H.Z., He, Y., Feng, T., 2018. Effective network of deep brain stimulation of subthalamic nucleus with bimodal positron emission tomography/functional magnetic resonance imaging in Parkinson's disease. CNS Neurosci. Ther. 24, 135–143.

Chung, C.Y., Koprich, J.B., Siddiqi, H., Isacson, O., 2009. Dynamic changes in presynaptic and axonal transport proteins combined with striatal neuroinflammation precede dopaminergic neuronal loss in a rat model of AAV alpha-synucleinopathy. J. Neurosci. 29, 3365–3373.

Coune, P.G., Craveiro, M., Gaugler, M.N., Mlynarik, V., Schneider, B.L., Aebischer, P., Gruetter, R., 2013. An in vivo ultrahigh field 14.1 T (1) H-MRS study on 6-OHDA and alpha-synuclein-based rat models of Parkinson's disease: GABA as an early disease marker. NMR Biomed. 26, 43–50.

Crabbe, M., Van der Perren, A., Weerasekera, A., Himmelreich, U., Baekelandt, V., Van Laere, K., Casteels, C., 2018. Altered mGluR5 binding potential and glutamine concentration in the 6-OHDA rat model of acute Parkinson's disease and levodopa-induced dyskinesia. Neurobiol. Aging 61, 82–92.

Decressac, M., Mattsson, B., Lundblad, M., Weikop, P., Bjorklund, A., 2012. Progressive neurodegenerative and behavioural changes induced by AAV-mediated overexpression of alpha-synuclein in midbrain dopamine neurons. Neurobiol. Dis. 45, 939–953.

Dienel, G.A., Hertz, L., 2001. Glucose and lactate metabolism during brain activation. J. Neurosci. Res. 66, 824–838.

Dienel, G.A., Behar, K.L., Rothman, D.L., 2018. Cellular origin of [(18)F]FDG-PET imaging signals during ceftriaxone-stimulated glutamate uptake: astrocytes and neurons. Neuroscientist 24, 316–328.

Eckert, T., Tang, C., Eidelberg, D., 2007. Assessment of the progression of Parkinson's disease: a metabolic network approach. Lancet Neurol. 6, 926–932.

Edison, P., Ahmed, I., Fan, Z., Hinz, R., Gelosa, G., Ray Chaudhuri, K., Walker, Z., Turkheimer, F.E., Brooks, D.J., 2013. Microglia, amyloid, and glucose metabolism in Parkinson's disease with and without dementia. Neuropsychopharmacology 38, 938–949.

Gao, H.M., Kotzbauer, P.T., Uryu, K., Leight, S., Trojanowski, J.Q., Lee, V.M., 2008. Neuroinflammation and oxidation/nitration of alpha-synuclein linked to dopaminergic neurodegeneration. J. Neurosci. 28, 7687–7698.

Ghadery, C., Koshimori, Y., Coakeley, S., Harris, M., Rusjan, P., Kim, J., Houle, S., Strafella, A.P., 2017. Microglial activation in Parkinson's disease using [(18)F]-FEPPA. J. Neuroinflammation 14, 8.

Guo, L., Xiong, H., Kim, J.I., Wu, Y.W., Lalchandani, R.R., Cui, Y., Shu, Y., Xu, T., Ding, J.B., 2015. Dynamic rewiring of neural circuits in the motor cortex in mouse models of Parkinson's disease. Nat. Neurosci. 18, 1299–1309.

Huang, C., Mattis, P., Tang, C., Perrine, K., Carbon, M., Eidelberg, D., 2007. Metabolic brain networks associated with cognitive function in Parkinson's disease. Neuroimage 34, 714–723.

Iannaccone, S., Cerami, C., Alessio, M., Garibotto, V., Panzacchi, A., Olivieri, S., Gelsomino, G., Moresco, R.M., Perani, D., 2013. In vivo microglia activation in very early dementia with Lewy bodies, comparison with Parkinson's disease. Parkinsonism Relat. Disord. 19, 47–52.

Im, H.J., Hahm, J., Kang, H., Choi, H., Lee, H., Hwang do, W., Kim, E.E., Chung, J.K., Lee, D.S., 2016. Disrupted brain metabolic connectivity in a 6-OHDA-induced mouse model of Parkinson's disease examined using persistent homology-based analysis. Sci. Rep. 6, 33875.

Jang, D.P., Min, H.K., Lee, S.Y., Kim, I.Y., Park, H.W., Im, Y.H., Lee, S., Sim, J., Kim, Y.B., Paek, S.H., Cho, Z.H., 2012. Functional neuroimaging of the 6-OHDA lesion rat model of Parkinson's disease. Neurosci. Lett. 513, 187–192.

Koshimori, Y., Ko, J.H., Mizrahi, R., Rusjan, P., Mabrouk, R., Jacobs, M.F., Christopher, L., Hamani, C., Lang, A.E., Wilson, A.A., Houle, S., Strafella, A.P., 2015. Imaging striatal microglial activation in patients with Parkinson's disease. PLoS One 10, e0138721.

Lauwers, E., Beque, D., Van Laere, K., Nuyts, J., Bormans, G., Mortelmans, L., Casteels, C., Vercammen, L., Bockstael, O., Nuttin, B., Debyser, Z., Baekelandt, V., 2007. Non-invasive imaging of neuropathology in a rat model of alpha-synuclein overexpression. Neurobiol. Aging 28, 248–257.

Lo Bianco, C., Ridet, J.L., Schneider, B.L., Deglon, N., Aebischer, P., 2002. alpha-Synucleinopathy and selective dopaminergic neuron loss in a rat lentiviral-based model of Parkinson's disease. Proc. Natl. Acad. Sci. U. S. A. 99, 10813–10818.

Ma, Y., Johnston, T.H., Peng, S., Zuo, C., Koprich, J.B., Fox, S.H., Guan, Y., Eidelberg, D., Brotchie, J.M., 2015. Reproducibility of a Parkinsonism-related metabolic brain network in non-human primates: a descriptive pilot study with FDG PET. Mov. Disord. 30, 1283–1288.

Maia, S., Arlicot, N., Vierron, E., Bodard, S., Vergote, J., Guilloteau, D., Chalon, S., 2012. Longitudinal and parallel monitoring of neuroinflammation and neurodegeneration in a 6-hydroxydopamine rat model of Parkinson's disease. Synapse 66, 573–583.

Matthews, D.C., Lerman, H., Lukic, A., Andrews, R.D., Mirelman, A., Wernick, M.N., Giladi, N., Strother, S.C., Evans, K.C., Cedarbaum, J.M., Even-Sapir, E., 2018. FDG PET Parkinson's disease-related pattern as a biomarker for clinical trials in early stage disease. Neuroimage Clin. 20, 572–579.

McGeer, P.L., Itagaki, S., Tago, H., McGeer, E.G., 1988. Occurrence of HLA-DR reactive microglia in Alzheimer's disease. Ann. N. Y. Acad. Sci. 540, 319–323.

Meyer, P.T., Frings, L., Rucker, G., Hellwig, S., 2017. (18)F-FDG PET in parkinsonism: differential diagnosis and evaluation of cognitive impairment. J. Nucl. Med. 58, 1888–1898.

Moehle, M.S., West, A.B., 2015. M1 and M2 immune activation in Parkinson's Disease: foe and ally? Neuroscience 302, 59–73.

Mole, J.P., Subramanian, L., Bracht, T., Morris, H., Metzler-Baddeley, C., Linden, D.E., 2016. Increased fractional anisotropy in the motor tracts of Parkinson's disease suggests compensatory neuroplasticity or selective neurodegeneration. Eur. Radiol. 26, 3327–3335.

Niethammer, M., Tang, C.C., Vo, A., Nguyen, N., Spetsieris, P., Dhawan, V., Ma, Y., Small, M., Feigin, A., During, M.J., Kaplitt, M.G., Eidelberg, D., 2018. Gene therapy reduces Parkinson's disease symptoms by reorganizing functional brain connectivity. Sci. Transl. Med. 10.

Oliveras-Salva, M., Van der Perren, A., Casadei, N., Stroobants, S., Nuber, S., D'Hooge, R., Van den Haute, C., Baekelandt, V., 2013. rAAV2/7 vector-mediated overexpression of alpha-synuclein in mouse substantia nigra induces protein aggregation and

progressive dose-dependent neurodegeneration. Mol. Neurodegener. 8, 44.
Ory, D., Postnov, A., Koole, M., Celen, S., de Laat, B., Verbruggen, A., Van Laere, K., Bormans, G., Casteels, C., 2016. Quantification of TSPO overexpression in a rat model of local neuroinflammation induced by intracerebral injection of LPS by the use of [(18)F]DPA-714 PET. Eur. J. Nucl. Med. Mol. Imaging 43, 163–172.
Peelaerts, W., Bousset, L., Van der Perren, A., Moskalyuk, A., Pulizzi, R., Giugliano, M., Van den Haute, C., Melki, R., Baekelandt, V., 2015. alpha-Synuclein strains cause distinct synucleinopathies after local and systemic administration. Nature 522, 340–344.
Poewe, W., Seppi, K., Tanner, C.M., Halliday, G.M., Brundin, P., Volkmann, J., Schrag, A.E., Lang, A.E., 2017. Parkinson disease. Nat. Rev. Dis. Primers 3, 17013.
Ransohoff, R.M., 2016. How neuroinflammation contributes to neurodegeneration. Science 353, 777–783.
Sanchez-Guajardo, V., Febbraro, F., Kirik, D., Romero-Ramos, M., 2010. Microglia acquire distinct activation profiles depending on the degree of alpha-synuclein neuropathology in a rAAV based model of Parkinson's disease. PLoS One 5, e8784.
Schindlbeck, K.A., Eidelberg, D., 2018. Network imaging biomarkers: insights and clinical applications in Parkinson's disease. Lancet Neurol. 17, 629–640.
Shimo, Y., Wichmann, T., 2009. Neuronal activity in the subthalamic nucleus modulates the release of dopamine in the monkey striatum. Eur. J. Neurosci. 29, 104–113.
Spangler-Bickell, M.G., de Laat, B., Fulton, R., Bormans, G., Nuyts, J., 2016. The effect of isoflurane on (18)F-FDG uptake in the rat brain: a fully conscious dynamic PET study using motion compensation. EJNMMI Res. 6, 86.
Takkinen, J.S., Lopez-Picon, F.R., Al Majidi, R., Eskola, O., Krzyczmonik, A., Keller, T., Loyttyniemi, E., Solin, O., Rinne, J.O., Haaparanta-Solin, M., 2017. Brain energy metabolism and neuroinflammation in ageing APP/PS1-21 mice using longitudinal (18)F-FDG and (18)F-DPA-714 PET imaging. J. Cereb. Blood Flow Metab. 37, 2870–2882.
Terada, T., Yokokura, M., Yoshikawa, E., Futatsubashi, M., Kono, S., Konishi, T., Miyajima, H., Hashizume, T., Ouchi, Y., 2016. Extrastriatal spreading of microglial activation in Parkinson's disease: a positron emission tomography study. Ann. Nucl. Med. 30, 579–587.
Theodore, S., Cao, S., McLean, P.J., Standaert, D.G., 2008. Targeted overexpression of human alpha-synuclein triggers microglial activation and an adaptive immune response in a mouse model of Parkinson disease. J. Neuropathol. Exp. Neurol. 67, 1149–1158.
Tillerson, J.L., Cohen, A.D., Philhower, J., Miller, G.W., Zigmond, M.J., Schallert, T., 2001. Forced limb-use effects on the behavioral and neurochemical effects of 6-hydroxydopamine. J. Neurosci. 21, 4427–4435.
Toth, M., Little, P., Arnberg, F., Haggkvist, J., Mulder, J., Halldin, C., Gulyas, B., Holmin, S., 2016. Acute neuroinflammation in a clinically relevant focal cortical ischemic stroke model in rat: longitudinal positron emission tomography and immunofluorescent tracking. Brain Struct. Funct. 221, 1279–1290.
Turkheimer, F.E., Rizzo, G., Bloomfield, P.S., Howes, O., Zanotti-Fregonara, P., Bertoldo, A., Veronese, M., 2015. The methodology of TSPO imaging with positron emission tomography. Biochem. Soc. Trans. 43, 586–592.
Van der Perren, A., Macchi, F., Toelen, J., Carlon, M.S., Maris, M., de Loor, H., Kuypers, D.R., Gijsbers, R., Van den Haute, C., Debyser, Z., Baekelandt, V., 2015a. FK506 reduces neuroinflammation and dopaminergic neurodegeneration in an alpha-synuclein-based rat model for Parkinson's disease. Neurobiol. Aging 36, 1559–1568.
Van der Perren, A., Toelen, J., Casteels, C., Macchi, F., Van Rompuy, A.S., Sarre, S., Casadei, N., Nuber, S., Himmelreich, U., Osorio Garcia, M.I., Michotte, Y., D'Hooge, R., Bormans, G., Van Laere, K., Gijsbers, R., Van den Haute, C., Debyser, Z., Baekelandt, V., 2015b. Longitudinal follow-up and characterization of a robust rat model for Parkinson's disease based on overexpression of alpha-synuclein with adeno-associated viral vectors. Neurobiol. Aging 36, 1543–1558.
Varnas, K., Cselenyi, Z., Jucaite, A., Halldin, C., Svenningsson, P., Farde, L., Varrone, A., 2019. PET imaging of [(11)C]PBR28 in Parkinson's disease patients does not indicate increased binding to TSPO despite reduced dopamine transporter binding. Eur. J. Nucl. Med. Mol. Imaging 46, 367–375.
Walker, Z., Gandolfo, F., Orini, S., Garibotto, V., Agosta, F., Arbizu, J., Bouwman, F., Drzezga, A., Nestor, P., Boccardi, M., Altomare, D., Festari, C., Nobili, F., 2018. Clinical utility of FDG PET in Parkinson's disease and atypical parkinsonism associated with dementia. Eur. J. Nucl. Med. Mol. Imaging 45, 1534–1545.
Wang, Y., Yue, X., Kiesewetter, D.O., Niu, G., Teng, G., Chen, X., 2014. PET imaging of neuroinflammation in a rat traumatic brain injury model with radiolabeled TSPO ligand DPA-714. Eur. J. Nucl. Med. Mol. Imaging 41, 1440–1449.
Wienhard, K., 2002. Measurement of glucose consumption using [(18)F]fluorodeoxyglucose. Methods 27, 218–225.
Wu, C., Li, F., Niu, G., Chen, X., 2013. PET imaging of inflammation biomarkers. Theranostics 3, 448–466.
Zimmer, E.R., Parent, M.J., Souza, D.G., Leuzy, A., Lecrux, C., Kim, H.I., Gauthier, S., Pellerin, L., Hamel, E., Rosa-Neto, P., 2017. [(18)F]FDG PET signal is driven by astroglial glutamate transport. Nat. Neurosci. 20, 393–395.